PLY-BY-PLY DELAMINATION MORPHOLOGY IN COMPOSITE LAMINATES UNDER LOW-VELOCITY IMPACT

M. Francesca Pernice[1], Andrew T. Rhead[1]

[1]Department of Mechanical Engineering, University of Bath, Claverton Down, Bath, BA2 7AY, UK
Emails: M.F.Pernice@bath.ac.uk A.T.Rhead@bath.ac.uk

Keywords: impact damage, delamination, mechanical testing, ply blocking, damage resistance

Abstract
The residual strength of composite laminates following low-velocity impact is affected by the location and size of individual delaminations. This study presents a first step towards an empirical model for the impact damage morphology of individual delaminations. To this end, the total mismatch angle, defined as the sum over the full stacking sequence of the mismatch angle at each interface, is used to categorize the potential for delamination. Impact tests have been conducted on specimens with various different stacking sequences, selected to have a variety of different total mismatch angles. Impact tests were conducted at increasing impact energies, to evaluate the effect of energy level on individual delamination size derived from non-destructive inspections. Results indicate that the morphology of individual delaminations depends solely on the fibre orientation of the bounding plies and is independent of overall stacking sequence of the laminate, ply-percentages, the through-the-thickness location of the delamination within the laminate and impact energy. The extent of delamination at each interface is significantly influenced by impact energy and the number of interfaces available for delamination.

1. Introduction

Low-velocity impact of composite laminates produces a complex damage morphology, comprising delaminations, intra-ply cracks and fibre failure, which can lead to drastically reduced residual strength [1, 2]. The damage mechanism leading to this complex damage pattern is difficult to investigate. Moreover, the damage morphology resulting from an impact event on a composite laminate depends on a number of different parameters, such as stacking sequence, laminate thickness, ply thickness, target and impactor geometry, impact energy and support conditions. Results obtained for a specific set of values for these parameters cannot be assumed to be valid for a different configuration, resulting in a vast number of potential impact scenarios. Current analytical modelling approaches [3, 4] for composite laminates are not able to determine the size of individual delaminations at each ply interface, information that is required to predict sublaminate buckling-driven delamination failures in compression after impact scenarios. As a consequence, the design of composite structures relies on oversizing of components that are vulnerable to impact, to allow for the reduced strength.

The aim of this study is to take a first step towards developing an empirical model for prediction of individual delamination sizes resulting from low-velocity impact of a composite laminate with a generic stacking sequence. To this end, damage resulting from low-velocity impact of carbon fibre/epoxy composite laminates with a variety of stacking sequences was investigated. Impact tests were performed at different energies and the morphology and growth of delamination was evaluated by C-scan. Preliminary experimental results are reported in this paper.

2. Experimentation

2.1. Stacking Sequences Selection

Low-velocity impact tests were conducted on specimens with different stacking sequences, at various energy levels. A variety of stacking sequences were selected to investigate the effect of the through-thickness location of an interface and fibre orientations of the bounding plies on the extent and shape of delamination at individual interfaces. Fibre orientations were limited to the standard industrial 0°, ±45°, 90° angles. To maximise the data gathered from each test, a circular test window was employed during low-velocity impact tests. For quasi-isotropic laminates, the rotational symmetry of the laminate and the circular boundary of the test window means that damage morphologies for four stacking sequences are produced with each impact test (see "Rotated" stacking sequences in Table 1). For instance, a test on a specimen with stacking sequence $[(+45°/0°/-45°/90°)_2]_S$ provides a damage morphology which, if rotated by +45°, corresponds to the damage morphology in a specimen with stacking sequence $[(90°/+45°/0°/-45°)_2]_S$.

Stacking sequences selected for testing were classified according to the sum over the full stacking sequence of the mismatch angle between fibre orientations at each interface. The total mismatch angle provides a measure of ply "blocking" or ply "dispersion" within a stacking sequence (which has been postulated to affect post impact strength [5]) and is used to group stacking sequences which are expected to have a similar response to an impact event. Fig. 1 shows a histogram representing the frequency of

Table 1. Quasi-isotropic and zero-dominated symmetric stacking sequences.

Basic sequence *A*: $+45°/0°/-45°/90°$			
A-Lam	$[(+45°/0°/-45°/90°)_2]_S$		
Rotated	$[(90°/+45°/0°/-45°)_2]_S$	$[(-45°/90°/+45°/0°)_2]_S$	$[(0°/-45°/90°/+45°)_2]_S$
*A*0-Lam	$[+45°/0°/-45°/90°/+45°/0°/-45°/\mathbf{0}°]_S$		
A-Ply	$[+45°_2/0°_2/-45°_2/90°_2]_S$		
Rotated	$[90°_2/+45°_2/0°_2/-45°_2]_S$	$[-45°_2/90°_2/+45°_2/0°_2]_S$	$[0°_2/-45°_2/90°_2/+45°_2]_S$
*A*0-Ply	$[+45°_2/0°_2/-45°_2/90°/\mathbf{0}°]_S$		
A-OI	$[(+45°/0°)_2/(-45°/90°)_2]_S$		
Rotated	$[(90°/+45°)_2/(0°/-45°)_2]_S$	$[(-45°/90°)_2/(+45°/0°)_2]_S$	$[(0°/-45°)_2/(90°/+45°)_2]_S$
*A*0-OI	$[(+45°/0°)_2/(-45°/90°)/(-45°/\mathbf{0}°)]_S$		
Basic sequence *B*: $+45°/-45°/0°/90°$			
B-Lam	$[(+45°/-45°/0°/90°)_2]_S$		
Rotated	$[(90°/0°/+45°/-45°)_2]_S$	$[(-45°/+45°/90°/0°)_2]_S$	$[(0°/90°/-45°/+45°)_2]_S$
*B*0-Lam	$[+45°/-45°/0°/90°/+45°/-45°/0°/\mathbf{0}°]_S$		
B-Ply	$[+45°_2/-45°_2/0°_2/90°_2]_S$		
Rotated	$[90°_2/0°_2/+45°_2/-45°_2]_S$	$[-45°_2/+45°_2/90°_2/0°_2]_S$	$[0°_2/90°_2/-45°_2/+45°_2]_S$
*B*0-Ply	$[+45°_2/-45°_2/0°_2/90°/\mathbf{0}°]_S$		
B-OI	$[(+45°/-45°)_2/(0°/90°)_2]_S$		
Rotated	$[(90°/0°)_2/(+45°/-45°)_2]_S$	$[(-45°/+45°)_2/(90°/0°)_2]_S$	$[(0°/90°)_2/(-45°/+45°)_2]_S$
*B*0-OI	$[(+45°/-45°)_2/(0°/90°)/(0°/\mathbf{0}°)]_S$		

Excerpt from ISBN 978-3-00-053387-7

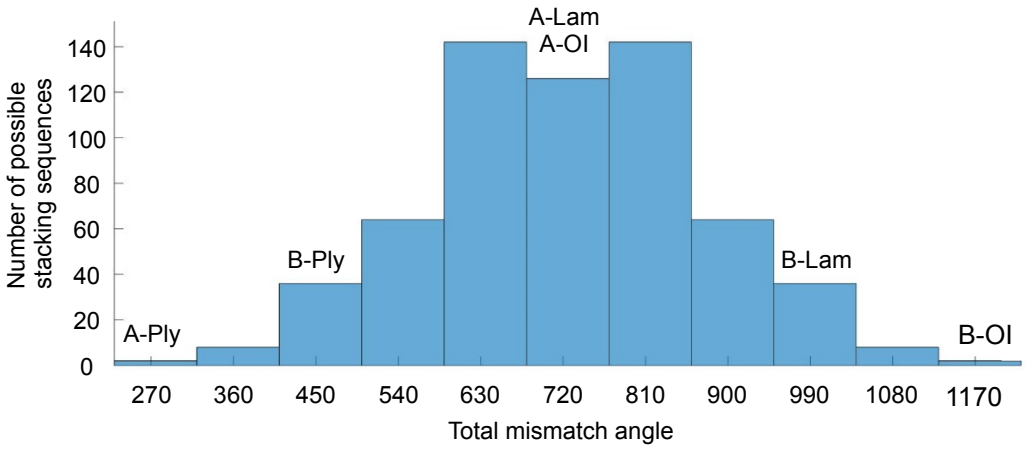

Figure 1. Classification of 16-ply quasi-isotropic stacking sequences based on the total sum of the mismatch angle between fibre orientations in adjacent plies.

occurrence of 16-ply quasi-isotropic symmetric stacking sequences with a particular total mismatch angle. The histogram was obtained using an equal number of plies with 0°, ±45° and 90° fibre orientations. Thanks to the rotational symmetry of the impact window used during testing, only stacking sequences having +45° plies on the outer surfaces were considered.

Stacking sequences selected for testing were obtained using two sequences of 4 plies, identified as basic sequence *A* and basic sequence *B* in Table 1. In sequence *A*, the mismatch between the fibre angle in two adjacent plies is always 45°. Sequence *B* has two interfaces (+45°/ − 45° and 0°/90°) with a mismatch angle of 90° between adjacent plies and only one 45° mismatch angle at the −45°/0° interface. Six 16-ply, quasi-isotropic, symmetric stacking sequences were obtained from the two basic sequences, *A* and *B*, and are shown in Table 1. For each one of them, the table shows the layups used for testing, identified as *A*-Lam, *A*-Ply, etc. and the rotated stacking sequences obtained by +45° rotations ("Rotated" stacking sequences in Table 1). All stacking sequences and ply blocks from left to right are written from the bottom to the top surface of the specimen. Stacking sequences *A*-Lam and *B*-Lam were obtained by repeating the basic sequences, *A* or *B*, twice, e. g. $[(+45°/0°/-45°/90°)_2]_S$ for *A*-Lam. The stacking sequences *A*-Ply and *B*-Ply were obtained by repeating each ply twice, e. g. $[+45°_2/0°_2/-45°_2/90°_2]_S$ for *A*-Ply. The outer eight plies in the stacking sequences *A*-Ply and *B*-Ply have the same sequence of interfaces as the outer 4-ply block in the corresponding stacking sequences *A*-Lam and *B*-Lam. Comparison of results obtained from these two pairs of corresponding layups (*A*-Lam and *A*-Ply, *B*-Lam and *B*-Ply) allows the effect of ply thickness and through-thickness interface position to be investigated. Stacking sequences *A*-OI and *B*-OI were obtained by splitting each basic ply sequence into its two outermost and two innermost plies, (e. g. +45°/0° and −45°/90° for the basic sequence *A*) and then repeating each pair e. g. $[(+45°/0°/+45°/0°/-45°/90°/-45°/90°)]_S$ for *A*-OI. The total mismatch angle of the quasi-isotropic stacking sequences tested in this study is shown in Fig. 1.

Zero-dominated stacking sequences, identified as *A*0-Lam, *A*0-Ply, etc. in Table 1, were also tested. These were obtained from the corresponding quasi-isotropic layups by replacing the two innermost 90° plies with two 0° plies, shown in bold in Table 1. The quasi-isotropic and the corresponding zero-

Excerpt from ISBN 978-3-00-053387-7

Table 2. Non-symmetric stacking sequences.

ID	Layup
NS 1	$[+45°/-45°/0°/90°/90°/0°/-45°/+45°/-45°/+45°/90°/0°/0°/90°/+45°/-45°]$
NS 2	$[+45°/-45°/-45°/+45°/0°/90°/90°/0°/90°/0°/0°/90°/-45°/+45°/+45°/-45°]$
NS 3	$[+45°/-45°/-45°/+45°/0°/90°/90°/0°/-45°/45°/45°/-45°/90°/0°/0°/90°]$
NS 4	$[+45°/-45°/-45°/+45°/0°/90°/90°/0°/0°/90°/90°/0°/+45°/-45°/-45°/+45°]$
NS 5	$[+45°/0°/-45°/90°]_4$

dominated stacking sequences have the same near surface ply stacks (Table 1), allowing the effect of ply-percentage to be investigated.

Similarly, specimens with non-symmetric stacking sequences were tested to evaluate the influence of the entire stacking sequence on individual delamination shape. These stacking sequences are shown in Table 2 and identified as *NS* 1 to *NS* 5.

2.2. Specimens Material and Manufacturing

Specimens were obtained from 230 mm-wide and 170 mm-long panels, made using T800/M21 carbon fibre/epoxy prepreg. Two panels were made for each stacking sequence. The panels were cured in an autoclave, according to the curing cycle recommended by the material manufacturer. Two specimens were obtained from each of the manufactured panels by trimming the edges of each panel and cutting them in half. Specimens were nominally 150 mm long (0° fibre direction) and 100 mm wide (90° fibre direction) [6], with an average cured thickness of 4.08 mm.

2.3. Test Procedure and Inspection Methods

Low-velocity impact tests were conducted at different energies, using an Instron dynatup 9250 drop weight impact tower, equipped with a 16 mm hemispherical tup. Tests were conducted according to the ASTM Standard [6], with the exception that a circular test window of diameter of 75 mm was employed. Tests were performed at impact energies varying between 6 J and 24 J in 6 J steps on specimens with quasi-isotropic stacking sequences, and at 18 J on specimens with zero-dominated and non-symmetric stacking sequences. For each non-symmetric stacking sequence, two specimens were impacted, one on the top surface (on the right hand side in Table 2) and one on the bottom surface (on the left hand side in Table 2). One test was conducted for each test configuration (impact energy and stacking sequence). The morphology of impact damage was inspected using an Ultrasonic Sciences Ltd. C-scan system, equipped with a 35 MHz probe.

3. Results

Figs. 2, 3, 4 and 5 show C-scan images of the non-impact surface of the specimens. Fibre orientations are indicated in the figures. Each figure compares delaminations in specimens containing the same near surface ply stacks regardless of the specific stacking sequence of the laminate and the through-the-thickness position of the interface. In each figure, the same colour represents an interface between two plies with specific fibre orientations.

In Fig. 2, a sequence of images of specimens with stacking sequences *A*-Lam and *A*-Ply tested at in-

Excerpt from ISBN 978-3-00-053387-7

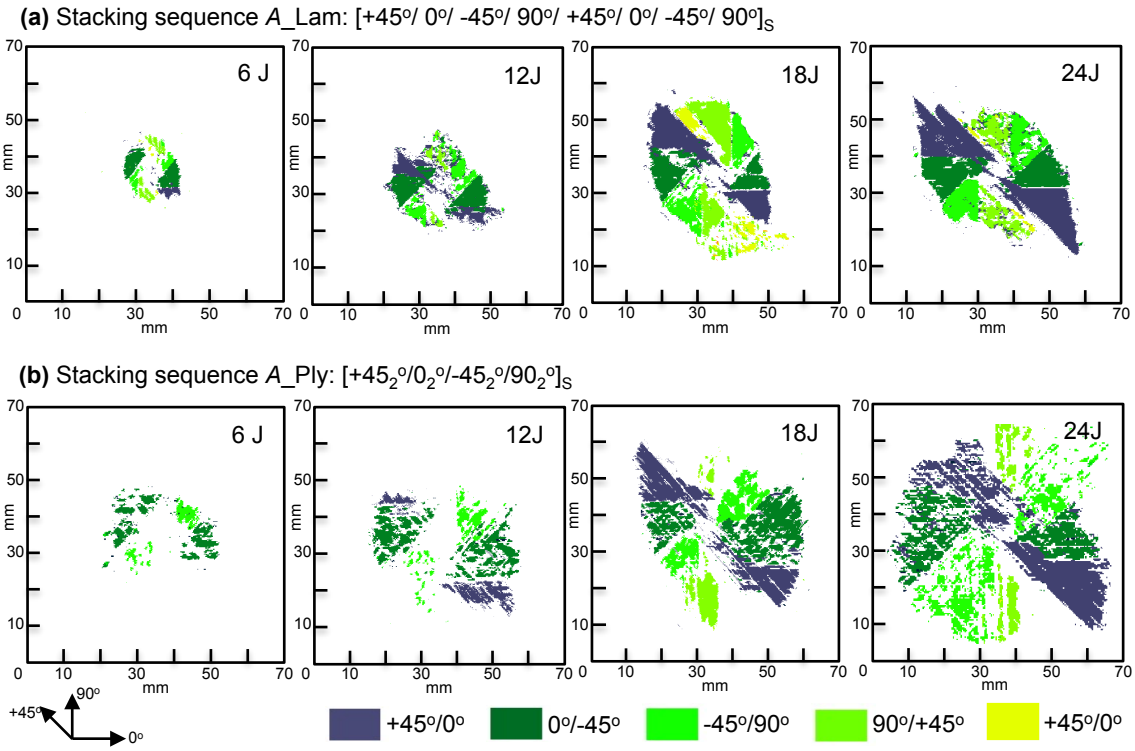

Figure 2. C-scan images of the non-impact surface of specimens with stacking sequence *A*-Lam (a) and *A*-Ply (b) tested at different impact energy.

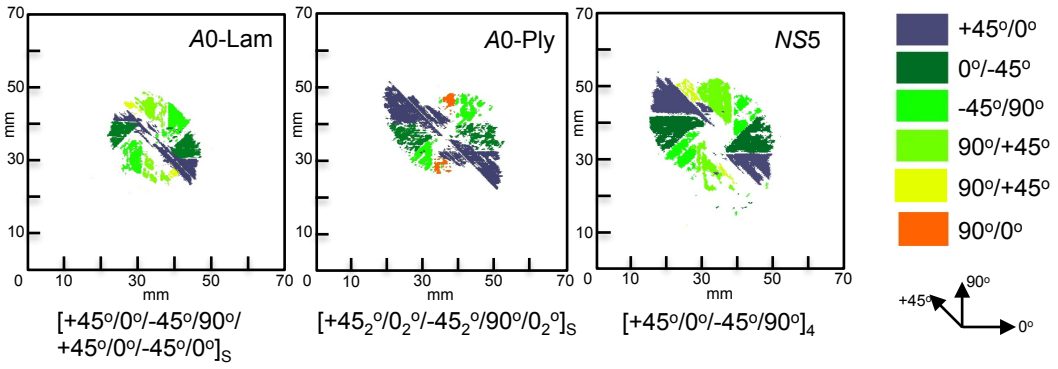

Figure 3. C-scan images of the non-impact surface of specimens with stacking sequence *A*0-Lam, *A*0-Ply and *NS* 5 tested at 18 J.

creasing energy levels in the range from 6 – 24 J (indicated in the figure) is shown. Note that in trial tests, impact below 6 J produced no detectable delamination damage and for impact energies greater than 24 J delamination reached the boundary of the circular test window, invalidating the test. Therefore, impact energy for all tests was limited to 24 J. Delaminations shown in Fig. 2 correspond to interfaces in the outer $+45°/0°/-45°/90°$ ply stack in each laminate. Delaminations size is shown to increase with increasing energy. Fig. 3 shows delaminations in this same ply stack in specimens with stacking sequences *A*0-Lam, *A*0-Ply and *NS* 5, after an 18 J impact. In Figs. 4(a-c), delaminations in the $+45°/-45°/-45°/+45°$ ply stack near the non-impact surface (left hand side in Table 2) in speci-

Excerpt from ISBN 978-3-00-053387-7

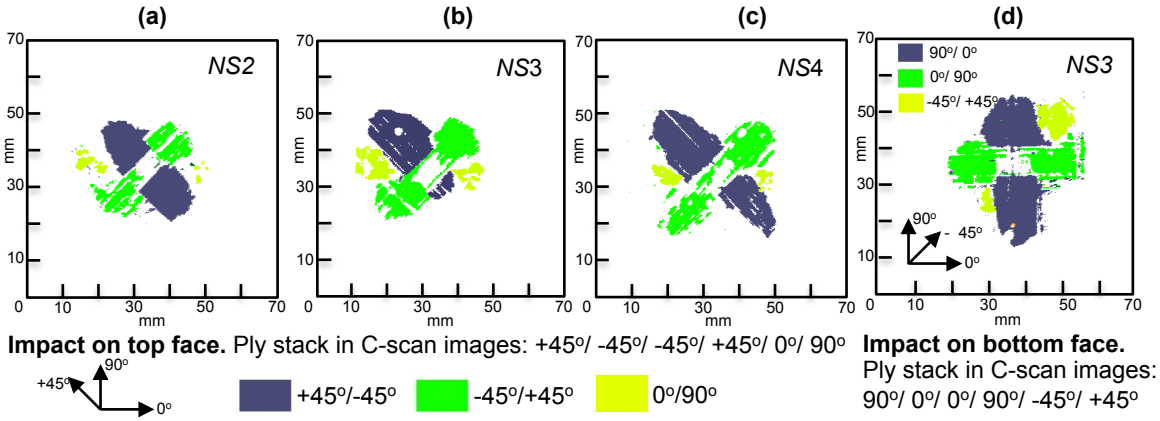

Figure 4. C-scan images of the non-impact surface of specimens with non-symmetric stacking sequences *NS* 2, *NS* 3 and *NS* 4 tested at 18 J.

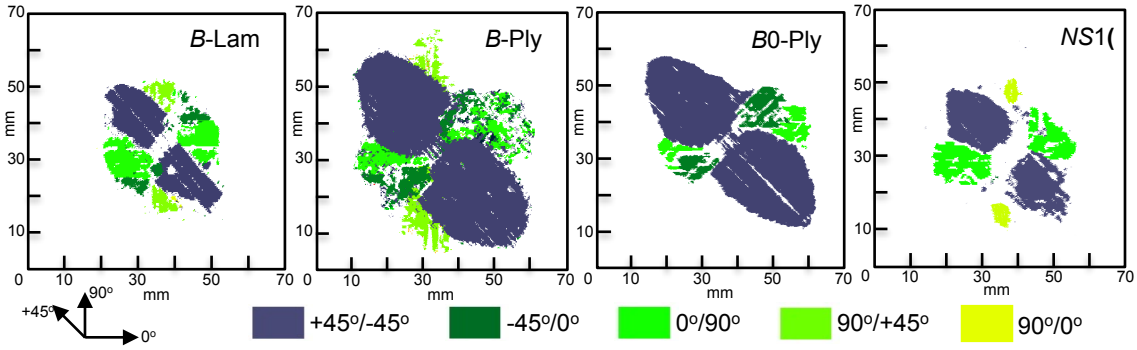

Figure 5. C-scan images of the non-impact surface of specimens with stacking sequence *B*-Lam, *B*-Ply, *B*0-Ply and *NS* 1 after impact at 18 J.

mens with non-symmetric stacking sequences *NS* 2, *NS* 3 and *NS* 4 impacted on the top face (right hand side in Table 2) are shown. The image in Fig. 4(d) shows delaminations in a specimen with stacking sequence *NS* 3 impacted on the bottom face (left hand side in Table 2). The ply stack shown in this case is 90°/0°/0°/90° (right hand side in Table 2) and corresponds to a 45° rotation of the ply stack in Figs. 4(a-c). Fig. 5 compares the delaminations in a +45°/ – 45°/0°/90° ply stack in specimens with stacking sequences *B*-Lam, *B*-Ply, *B*0-Lam and *NS* 1 after impact at 18 J. Similar damage patterns were obtained for stacking sequences *A*-OI, *B*-OI, *A*0-OI and *B*0-OI and are omitted for brevity. C-scan volume files and images for all specimens are available from [7].

4. Discussion

A ply-by-ply comparison of delaminations in specimens with the same ply stack near the non-impact surface tested at increasing energies shows that increasing impact energy creates larger delaminations (Fig. 2). However, Fig. 2 also shows that the delamination boundary (but not extent) at each ply interface is the same, independent of impact energy. For example, for all images in Fig. 2(a) the delamination at the first interface near the non-impacted surface, +45°/0°, is elongated along the +45° fibre orientation of the lower ply at the interface and is bounded by intra-ply cracks at +45° and 0°. With increasing impact

Excerpt from ISBN 978-3-00-053387-7

energy, this delamination grows along the +45° fibre direction of the lower ply bounding the interface. This behaviour was replicated at all other interfaces. In fact, in the images in Figs. 2(a) and (b), the delamination at the $0°/-45°$ interface grows along the 0° fibre direction of the lower bounding ply. Similarly, the $-45°/90°$ interface delamination propagates along the −45° fibre direction in the lower ply at the interface. A comparison of Figs. 2(a) and (b), shows that if ply thickness is effectively doubled (compare the outer 4 plies of *A*-Lam to the outer 8 plies of *A*-Ply in Table 1) delamination shape remains consistent, with each delamination still being bounded by intra-ply cracks aligned with the orientation of the bounding plies. Delamination growth with increasing impact energy is again in the direction of the lower ply at the interface. The same comparison of Figs. 2(a) and (b) also demonstrates that delamination shape is independent of the through-thickenss position of the ply stack.

Fig. 3 compares symmetric zero-dominated (*A*0-Lam and *A*0-Ply) and non-symmetric (*NS*5, impacted on the top face, right hand side as shown in Table 2) stacking sequences with the same near surface plies near the non-impact surface as in Fig. 2. Comparing these results to those in the quasi-isotropic stacking sequences in Fig. 2 shows that the shape of individual delaminations and bounding intra-ply cracks remains consistent in the $+45°/0°/-45°/90°$ ply stack and is thus independent of laminate symmetry and varied ply-percentages.

Fig. 4 allows comparison of non-symmetric laminates subject to 18 J impacts. The C-scan images shown capture delamination in the left hand end of sequences *NS*2 and *NS*4 and both ends of *NS*3 (Table 2). Fig. 4(d) shows a C-scan image of the right hand end of *NS*3, in a specimen impacted on the bottom surface (left hand side in Table 2). In all cases, the images show the non-impact surface. Comparison of the images shows that the shapes of the ply-by-ply delaminations are consistent across specimens with different overall stacking sequences and delamination remains bounded by intra-ply cracks aligned with the orientation of adjacent plies. Comparison of delaminations in the $90°/0°/0°/90°$ ply stack in Fig. 4(d) rotated by 45° with the $+45°/-45°/-45°/+45°$ ply stack in Figs. 4(a-c) shows that impact of quasi-isotropic laminates is rotationally symmetric.

Images in Fig. 5 indicate that the delamination boundary independence, noted in specimens obtained from the basic sequence *A*, also hold for stacking sequences constructed from basic sequence *B*. Delamination morphology is again independent of symmetry of the stacking sequence and ply-percentage.

The extent of delamination was found to be greater in stacking sequences with lower total mismatch angle ("blocked" stacking sequences *A*-Ply and *B*-Ply) compared with stacking sequences with greater total mismatch angle ("dispersed" stacking sequences *A*-Lam and *B*-Lam), see Figs. 2 and 5. This result is due to the lower number of interfaces of dissimilar fibre orientations available for delamination in the blocked stacking sequences

Overall it can be concluded that the shape of the delamination at each interface is characteristic of the fibre orientation in the plies bounding the delamination and does not depend on the stacking sequence or the through-the-thickness location of the interface in the laminate. As it has been noted previously [5, 8], it is postulated that delamination is bounded by intra-ply cracks in the adjacent plies and it is created by impingement of a strip of fibres, released from the upper ply by intra-ply cracks, onto the lower ply which then peels away from the upper ply in the fibre direction of the lower ply.

5. Concluding remarks

Low-velocity impact tests ranging from 6 to 24 J were conducted on specimens with different stacking sequences obtained from two basic sequences of 4 plies, $(+45°/0°/-45°/90°)$ and $(+45°/-45°/0°/90°)$. Quasi-isotropic, zero-dominated and non-symmetric stacking sequences variations were tested. The

Excerpt from ISBN 978-3-00-053387-7

shape and size of delamination at each interface in the near surface plies were inspected by C-scan of the specimens after testing.

For all stacking sequences tested it was found that the shape of the delamination at each interface, resulting from a low-velocity impact event, depends on the fibre orientation of the bounding plies at the interface. The shape of the delamination is shown to be independent of the overall stacking sequence of the laminate, the through-the-thickness location of the interface within the laminate and ply thickness. Tests conducted at increasing energy showed that, although delamination area increased, the shape of each delamination did not vary. The extent of delamination was found to increase with decreasing total mismatch angle in the stacking sequence at a given impact energy. Delamination propagation with increasing impact energy was always in the fibre direction of the lower bounding ply. Future work will see this study extended to thicker laminates and other composite material systems to validate the generality of the results obtained.

Acknowledgments

This paper is part of the EPSRC founded project "IMPACT". The authors would like to thank Prof. Stephen Hallett (University of Bristol) for allowing access to the impact test facilities in the laboratories of ACCIS, University of Bristol. Special thanks to Mr Chris Abbott and Mr James Barber (University of Bath) for their work on non-symmetric and zero-dominated stacking sequences.

References

[1] A. Sandhu, L. Glen, M. Doughty, and A. T. Rhead. X-Ray Computed Tomography of damage formation under in-situ loading. *Proceedings of the 20th International Conference on Composite Materials ICCM-20, Copenhagen, Denmark*, July 19-24 2015.

[2] E. Abisset, F. Daghia, X. C. Sun, M. R. Wisnom, and S. R. Hallett. Interaction of inter- and intralaminar damage in scaled quasi-static indentation tests: Part 1 – Experiments. *Composites: Part A*, 136:712–726, 2016.

[3] R. Olsson. Closed form prediction of peak load and delamination onset under small mass impact. *Composite Structures*, 59:341–349, 2003.

[4] R. Olsson, M. V. Donadon, and B. G. Falzon. Delamination threshold load for dynamic impact on plates. *International Journal of Solids and Structures*, 43:3124–3141, 2006.

[5] T. A. Sebaey, E. V. Gonzáles, C. S. Lopes, N. Blanco, P. Maimí, and J. Costa. Damage resistance and damage tolerance of dispersed CFRP laminates: Effect of the mismatch angle between plies. *Composite Structures*, 101:255–264, 2013.

[6] ASTM D7136/D7136M-15. Standard Test Method for Measuring the Damage Resistance of a Fiber-Reinforced Polymer Matrix Composite to a Drop-Weight Impact Event. In *Annual Book of ASTM Standards*, volume 15.03. American Society for Testing and Materials, 2015.

[7] A. Rhead. Imaging and probabilistic assessment of composite damage threats (IMPACT). *University of Bath*, http://doi.org/10.15125/BATH-00195, 2016.

[8] C. Bouvet, B. Castanie, M. Bizeul, and J. J. Barrau. Low velocity impact modelling in laminate composite panels with discrete interface elements. *International Journal of Solids and Structures*, 46(14-15):2809–2821, 2009.